Microchimica Acta (2022) 189: 326
https://doi.org/10.1007/s00604-022-05408-0

ORIGINAL PAPER

Electrochemical enzyme-based blood uric acid biosensor: new insight into the enzyme immobilization on the surface of electrode via poly-histidine tag

Amineh Mashkoori[1,2] · Ali Mostafavi[1] · Tayebeh Shamspur[1] · Masoud Torkzadeh-Mahani[3]

Received: 18 April 2022 / Accepted: 6 July 2022 / Published online: 10 August 2022

Abstract

In a new approach, we considered the special affinity between Ni and poly-histidine tags of recombinant urate oxidase to utilize Ni-MOF for immobilizing the enzyme. In this study, a carbon paste electrode (CPE) was modified by histidine-tailed urate oxidase (H-UOX) and nickel-metal–organic framework (Ni-MOF) to construct H-UOX/Ni-MOF/CPE, which is a rapid, sensitive, and simple electrochemical biosensor for UA detection. The use of carboxy-terminal histidine-tailed urate oxidase in the construction of the electrode allows the urate oxidase enzyme to be positioned correctly in the electrode. This, in turn, enhances the efficiency of the biosensor. Characterization was carried out by X-ray diffraction (XRD), energy-dispersive X-ray spectroscopy (EDX), Fourier transform infrared spectroscopy (FTIR), Brunauer–Emmett–Teller (BET), and field emission scanning electron microscopy (FE-SEM). At optimum conditions, the biosensor provided a short response time, linear response within 0.3–10 μM and 10–140 μM for UA with a detection limit of 0.084 μM, repeatability of 3.06%, and reproducibility of 4.9%. Furthermore, the biosensor revealed acceptable stability and selectivity of UA detection in the presence of the commonly coexisted ascorbic acid, dopamine, L-cysteine, urea, and glucose. The detection potential was at 0.4 V vs. Ag/AgCl.

Keywords Urate oxidase · Uric acid · Biosensor · Ni-MOF · Electrochemical detection · Differential pulse voltammetry · Histidine

Introduction

Elevated uric acid levels are the symptoms of gout, high cholesterol, hyperuricemia, obesity, Lesch-Nyhan syndrome, high cholesterol, enhanced alcohol consumption, cardiovascular disease, diabetes, and kidney disease [1, 2]. The amount of uric acid is determined via several analytical methods, ranging from the simple colorimetric methods using immobilized enzymes or commercially available enzymatic kits, flow-injection methods [3], and chemiluminescence and fluorometric methods [4–6], to the high-resolution separation methods, such as high-performance liquid chromatography and capillary electrophoresis [2, 7]. Electrochemical techniques, which have a higher sensitivity and faster detection ability than the previous methods, such as spectroscopy and HPLC [2, 8], are also used [4]. The presence of other substances in the sample matrix (e.g., ascorbic acid and dopamine), which oxidize easily, can cause interference in the process of uric acid determination in complex samples of biological origin. These interferences usually result in a reduction of selectivity in electroanalytical methods. Catalytically modified electrodes, on which the interferences of ascorbic acid and dopamine can be reduced or eliminated, can improve the selectivity of electrochemical uric acid determination [9–11]. For this purpose, enzymatic methods combined with electrochemical detection are preferred. Urate oxidase (UOX) is an uncommon oxidoreductase enzyme and part of a diagnostic kit that is used to determine the uric acid concentration in the blood, a very important clinical

✉ Masoud Torkzadeh-Mahani
mtmahani@gmail.com

[1] Department of Chemistry, Shahid Bahonar University of Kerman, Kerman, Iran

[2] Young Researchers Society, Shahid Bahonar University of Kerman, Kerman, Iran

[3] Department of Biotechnology, Institute of Science and High Technology and Environmental Sciences, Graduate University of Advanced Technology, Kerman, Iran

measurement [12, 13]. The UOX from *Aspergillus flavus* is mainly used to treat gout and hyperuricemia [12, 14]. It is more efficient than any other drug owing to the low incidence of hypersensibility reaction [15]. Many studies on UOX immobilization have been carried out for biosensor development [12, 16], where various procedures, including the use of metal–organic frameworks (MOFs) [17–19], have been used to immobilize enzymes.

MOFs generally comprise metal ion/cluster centers connected to organic linker molecules [20]. The synthesis of MOFs has received enormous attention in the last two decades thanks to their flexibility in constructing a large diversity of esthetically interesting structures, which may also be of great interest in a number of fields associated with porous materials [21].

Due to their tunable porosity, open cavities, high surface areas, and great chemical/thermal stability, MOFs have received and have found popularity in many fields such as catalysis, optics, electronics, gas adsorption, energy storage [19, 22, 23], drug delivery [20, 24, 25], and sensors [20, 26]. Also, MOFs are a very good choice for enzyme immobilization [19, 27]. Protein tags are an amino acid motif in protein that typically are found at the protein's N- or C-terminus, which are attached to proteins to facilitate easy detection and purification of expressed proteins. The poly-histidine tag is a widely used protein tag composed of 6–10 consecutive histidine amino acids at either terminus of the protein of interest. This His-tag bonds tightly with the immobilized metal ions since the side chain of histidine, imidazole, has a special binding affinity to immobilized divalent metal ions; nickel is the most frequently used, followed by cobalt, but other divalent metals are also employed. As a result, the desired protein can be bound tightly to the targeted immobilized metal ions (in this case, nickel) in a specific location and proper direction. With this targeted enzyme orientation, the enzyme's active site can be protected, and the enzyme can maintain its original activity [28].

In this research, a novel, sensitive, and selective uric acid biosensor was successfully constructed using an immobilized recombinant urate oxidase on the surface of Ni-MOF. Ni-MOF was generated by solvothermal reactions. The biosensor for uric acid detection was constructed using Ni-MOF as the enzyme retaining agent in the electrode. The presence of poly-histidine tail in the carboxy-terminal of recombinant urate oxidase would cause the enzyme to orient itself correctly on the electrode surface. Due to the high affinity between the histidine amino acid and Ni [29], histidine is bound to Ni in the Ni-MOF. After this interaction, the enzyme is linked to Ni-MOF in the proper direction, causing protection of its activity. Thus, the enzyme is retained in the electrode with excellent activity and stability. The new H-UOX/Ni-MOF/CPE was successfully applied to determine UA in the human serum sample. It revealed an excellent performance for quick determination of UA.

Experimental

Materials and apparatus

Uric acid was purchased from Alfa Aesar (Karlsruhe, Germany; https://www.alfa.com). 1,3,5-Benzenetricarboxylic acid, phosphoric acid, 2,2'-bipyridine, acetic acid, N, N-dimethylformamide, citric acid, sodium hydroxide, ascorbic acid, glucose, $Ni(NO3)_2$ $6H_2O$, and urea were provided by Merck (Darmstadt, Germany; https://www.Merk.com). Ethanol was procured from Ghadir Industries (Iran). Kanamycin and isopropyl β-D-1-thiogalactopyranoside (IPTG) were purchased from BioBasic Inc. Graphite powder was obtained from DAE JUNG (Korea). All other chemicals were obtained from Merck (NJ, USA; https://www.Merk.com).

The electrochemical determinations were performed using an Autolab PGSTAT 101 electrochemical system from Metrohm (Herisau, Switzerland; http://www.metrohm.com). The experimental parameters were controlled with Nova 1.11 software. A three-electrode configuration consisting of Ag/AgCl/KCl (3 M) as the reference, platinum wire as the axillary electrode, and H-UOX/Ni-MOF/CPE as the working electrode were applied for all voltammetry experiments. All pH investigations were performed by a Metrohm 827 pH meter (Herisau, Switzerland; http://www.metrohm.com). FTIR spectra were achieved by a Tensor 27 spectrometer. FE-SEM, EDX, and mapping images were achieved using field emission scanning electron microscopy (MIRA3, Tescan-Xmu, Czech Republic) equipped with an EDX analyzer. The crystalline structure of the Ni-MOF was investigated by an X-ray diffraction system (X'pert PRO diffractometer, Panalytical, Netherlands). The BET technique (BEL, BELSORP MINI II model, and Japan) was used to determine the nitrogen adsorption/desorption sample at 77 K. Ni nitrilotriacetic (Ni–NTA) chromatography columns were obtained from Invitrogen. Raman spectra were achieved by a TakRam N1-541 spectrometer.

Expression of UOX in *Escherichia coli*

Here, 7 µl of transformed *Escherichia coli* cells [30] was precultured in a 5-ml Luria Broth medium containing 50 µg/ml kanamycin, where the sample was incubated at 37 °C for 12 h in a shake flask with 250 rpm. Then, 1 ml of the precultured medium was added to 100 ml of terrific broth medium containing 0.3 mg/ml kanamycin. The mixture was incubated at 37 °C at 250 rpm until the OD600 of the medium reached 0.7. Next, to induce the recombinant protein's expression,

isopropyl-beta-Dthiogalactopyranoside (IPTG) was added to the medium at the final concentration of 1 mM. Ten hours after IPTG induction, the cells were harvested via centrifugation at 6000 rpm (4000 g) for 10 min. The supernatant was discarded, and the cell pellet was resuspended in an equal volume of lysis buffer (Tris HCL 50 mM PH = 7.8). Now, samples were sonicated thirteen times for 30 s on ice with 30 s break time. The cell lysate was centrifuged at 13,000 rpm (19,000 g) for 20 min. The clear supernatant (containing soluble protein) was collected.

Purification and concentration of UOX

UOX was purified by Ni–NTA-sepharose column according to the Invitrogen protocol [12, 31, 32], and the concentration of purified protein was determined by the Bradford method [33]. SDS-PAGE (sodium dodecyl sulfate–polyacrylamide gel electrophoresis) analysis of uricase was performed after purification to examine the purity. A total of 750 µl Bradford solution was used to reset the spectrometer to zero at 595 nm, and then the absorbances of the standards and samples were recorded at 595 nm. To generate the standard curve, we prepared several dilutions of the protein standard Bovine serum albumin. A standard curve was generated by plotting the average absorbance, where the amount of protein was determined for the sample using the standard curve.

Preparation of Ni-MOF

The Ni-MOF was synthesized as follows [34]: 0.211 g of 1,3,5 benzene tricarboxylic acid, 0.192 g of 2,2'-bipyridine, and 0.292 g of $Ni(NO_3)_2.6H_2O$ were mixed in 40 ml of DMF. This solution was placed in the oven at 120 °C for 4 h, then cooled to room temperature. The obtained solid Ni-MOF was collected through centrifugation, rinsed with DMF and C_2H_5OH, and dried in air at 60 °C for 12 h. Finally, the resulting crystals were calcinated at 135 °C for 2 h.

Fabrication of the modified CPE

The modified CPE was fabricated by mixing 0.095 g graphite powder, 0.050 g Ni-MOF, 2 µl urate oxidase enzyme, and paraffin oil. The mixture was well blended in a mortar for 20 min to obtain a homogenous paste and then packed in one end of a glass tube (3 mm inner diameter) with a copper wire as the electrical contact. The surface of the electrode became mirror-like when polished on a weighing paper just before use (Scheme 1).

Experimental procedure

Here, 10 ml of 100 µM UA in 0.5 M acetate buffer (pH 5.5) was transferred to the electrochemical cell. Then, the prepared electrode was placed in the solution, with UA determination performed by DPV. DP voltammograms (DPV) in all experiments were recorded from 0 to 0.8 V at a scan rate of 100 mV s^{-1}, pulse width of 50 ms, pulse amplitude of 50 mV, and step potential of 10 mV. The electrochemical performances of the H-UOX/Ni-MOF/CPE were examined using differential pulse voltammetry (DPV) and impedance analysis (EIS).

The quantification of UA in real samples

A human serum sample was chosen as a real sample for analysis using the standard addition method. Here, 1 ml of serum sample was mixed with 10 ml methanol before the measurement for deproteinization. After a 30-min centrifugation at 3000 rpm, supernatants were filtered and diluted. Then, specified amounts of UA were added to the sample (three times) to evaluate the recoveries. For UA measurement in each sample, the H-UOX/Ni-MOF/CPE was immersed in 10 ml of the prepared sample solution, and a DPV was obtained. The pulse width of 50 ms, pulse amplitude of 50 mV, and step potential of 10 mV, between 0 and 0.8 V, were used. According to Table 1, the obtained recoveries are satisfactory and illustrate that the proposed biosensor is suitable for measuring UA in biological samples with no considerable interference from coexists, including ascorbic acid, urea, glucose, dopamine, and L-cysteine.

Results and discussion

Ni-MOF characterization

Various techniques were used to characterize the Ni-MOF, including FE-SEM, BET, FT-IR, EDX, mapping, and XRD. Figure 1a(1–3) displays the FE-SEM images of the Ni-MOF, revealing the porous and spherical morphology with a diameter of about 7.46 µm. A high-magnification SEM image (Fig. 1a3) illustrates the presence of many pores on the inner wall of the hole and the surface. As can be seen in Fig. 1a, Ni-MOF revealed a uniform and porous nanostructure, providing a significant increase of effective area for enzyme loading, thus resulting in a good electrochemical response to uric acid. FT-IR studied the chemical structure of Ni-MOF. Figure S1 demonstrates the FTIR spectra of 2,2'bipyridine, 1,3,5 benzene tricarboxylic acid, and Ni-MOF. According to the FT-IR spectrum of 1,3,5-benzene tricarboxylic acid, the intense peak at 1721 cm^{-1} was attributed to C–O stretching vibration in free carboxylic acids (1760–1690 cm^{-1}). As can be seen, the intensity of this peak in the free acid linker was considerably higher than that of the Ni-MOF [35]. Also, the absorption band at 1362 cm^{-1} was ascribed to the C–O stretch of 1,3,5-benzene tricarboxylic acid. The FT-IR spectrum of the Ni-MOF reveals

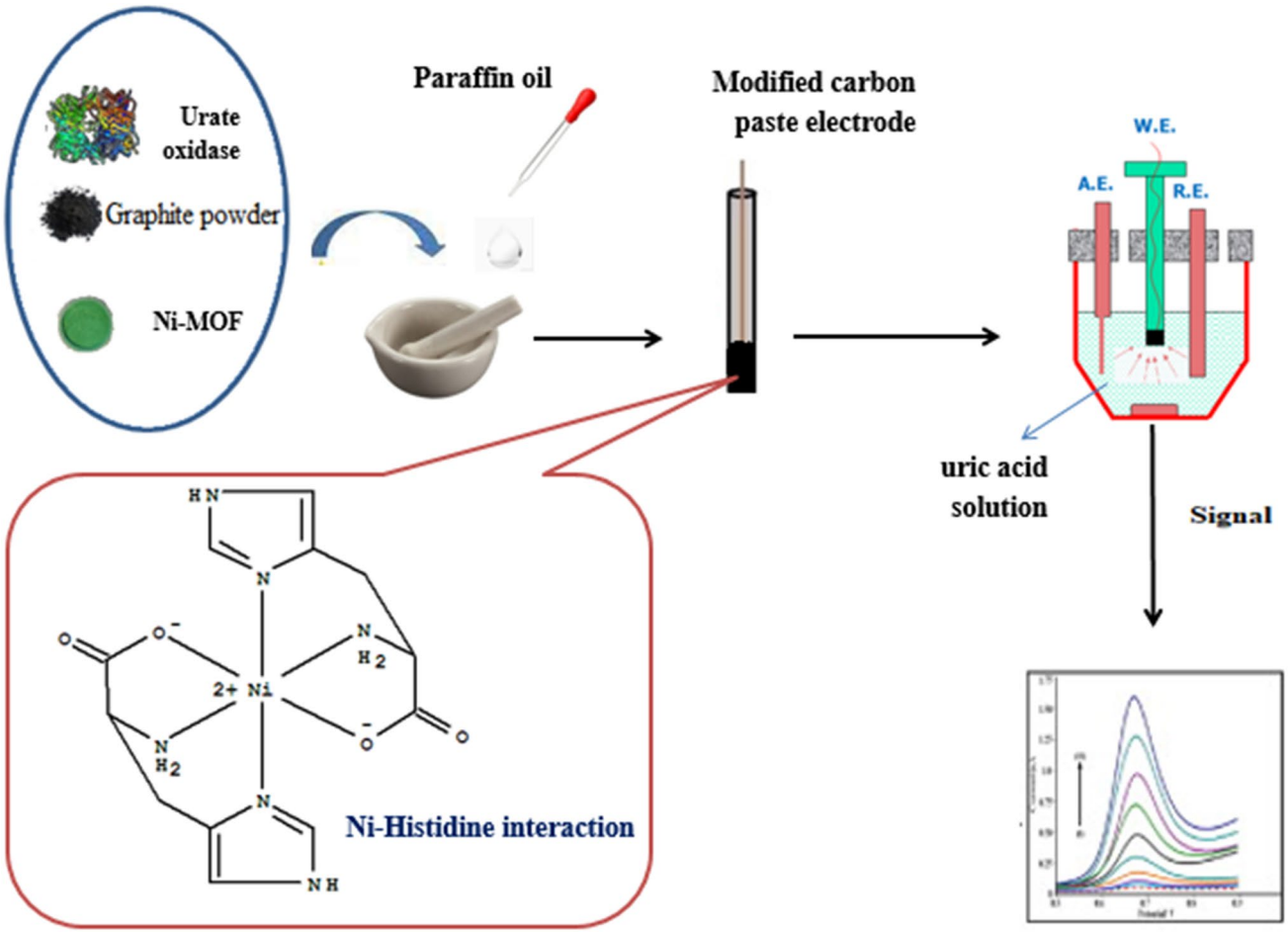

Scheme 1 The steps for construction of UOX biosensor

Table 1 Determination of UA in real sample

Sample	Added amount (μM)	Found amount (μM)	ELISA method result	Recovery
	0	4.69 ± 0.05	5.0	-
Serum	9	13.60 ± 0.90	nt	99
	40	46.29 ± 2	nt	104

nt not tested

characteristic peaks of 3387, 1130, 933, and 635 cm^{-1}, which are due to the OH stretching of 1,3,5-benzene tricarboxylic acid, C–O stretching of 1,3,5-benzene tricarboxylic acid, ring breathing of the C–C stretching of 2,2'–bipyridine, and C–C stretch of 1,3,5-benzenetricarboxylic acid, respectively. The peaks at 1370 and 1444 cm^{-1} are attributed to the incorporation of nitrogen, which is present in 2,2'-bipyridine, with nickel ions [34]. Also, the Ni-MOF spectra demonstrate a sharp absorption peak at 1611 cm^{-1}, illustrating the COOH groups in the 1,3,5-benzenetricarboxylic acid deprotonated due to reaction with nickel ions [35–37]. All characteristic bands associated with 2,2'-bipyridine and 1,3,5-benzenetricarboxylic acid were detected in the final spectrum, confirming the conjunction of Ni^{2+} ions with 2,2'-bipyridine and 1,3,5-benzenetricarboxylic acid. Furthermore, elemental mapping of Ni-MOF is demonstrated in Fig. 1b. According to the results, the final nanostructure consists of C, O, N, and Ni elements, which have a homogeneous distribution on the Ni-MOF. The homogeneous distribution of C, O, N, and Ni elements on the Ni-MOF is clearly illustrated by mapping images.

The XRD pattern inspected the structure crystallinity of Ni-MOF. Figure 1c indicates diffraction peaks located at 2θ = 11.660, 25.300, 26.962, 29.020, and 42.380 with cubic phase indexed to (0 -1 1), (2 0 2), (-1 0 3), (0 3 3), and (1 5 4), respectively. This can be used for measuring the crystalline size of Ni-MOF using the Scherer equation:

$$D\ 1/4\ k\ \lambda = \beta\ \cos\theta \quad (1)$$

The quantitative analysis based on Eq. (1) illustrated that the crystalline size of Ni-MOF is 8.1 nm. Furthermore, EDX

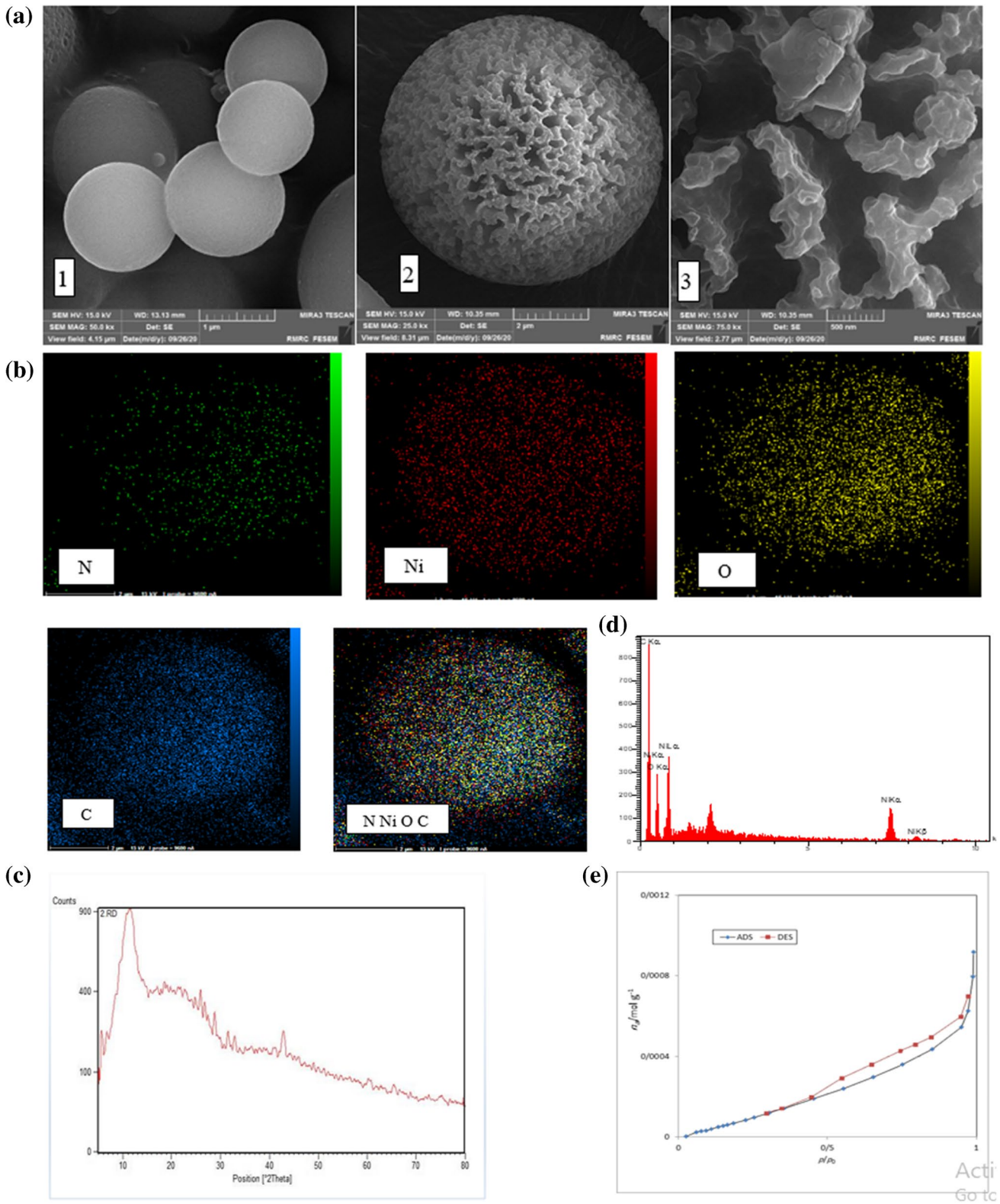

Fig.1 **a** FE-SEM images at different magnifications: × 50.0 k, × 25.0 k, and × 75.0 k. **b** Mapping images. **c** XRD pattern. **d** EDX pattern. **e** Nitrogen adsorption–desorption isotherm of the as-synthesized mesoporous Ni-MOF

spectroscopy was used to study the elemental composition of Ni-MOF (Fig. 1d).

Nitrogen adsorption/desorption isotherms of mesoporous Ni-MOF are displayed in Fig. 1e. According to the IUPAC classification, the adsorption isotherm of porous Ni-MOF is a type (III) isotherm, indicating a mesoporous structure with H_3-type hysteresis loop [38, 39]. Using the BET technique, the total pore volume and mean pore diameter of the mesoporous Ni-MOF were calculated as 0.030073 ± 0.0009 $cm^3\ g^{-1}$ and 15.443 ± 0.463 nm, respectively. Total pore volume was achieved from the amount of N_2 adsorbed at P/Po = 0.990. Accordingly, Ni-MOF can be used as an appropriate retaining agent for UOX due to its porous structure and Ni ions.

UOX/Ni-MOF characterization

To illustrate the interaction between UOX and Ni-MOF, Raman spectra of Ni-MOF and UOX/Ni-MOF were studied and shown in supplementary electronic materials (Fig. S2).

Enzyme purity and concentration

As indicated in Fig. S3, after purification, the protein was found as a single band on SDS-PAGE, and its molecular mass was approximately 34 kDa. The concentration of purified enzyme was 1.9 mg/ml for elution No. 2.

The electrochemical manner of the modified carbon paste electrode in UA measurement

Figure 2A illustrates DPV achieved after the determination of UA at CPE (curve a), H-UOX/CPE (curve b), and H-UOX/Ni-MOF/CPE (curve c) from an 80 µM UA in 0.50 M acetate buffer (pH 5.50) and H-UOX/Ni-MOF/CPE (curve d) from an 0.50 M acetate buffer (0 µM UA). In addition, cyclic voltammograms of H-UOX/CPE and H-UOX/Ni-MOF/CPE from an 80 µM UA in 0.50 M acetate buffer (pH 5.50) were investigated (Fig. S4). As seen, adding H-UOX to CPE leads to increasing signal and shifting potential. The peak current of the H-UOX/Ni-MOF/CPE was higher than that of H-UOX/CPE. By modifying the UOX/CPE with Ni-MOF, the sensitivity was significantly enhanced due to the electrocatalytic property of the Ni-MOF [46].

Study of scan rate effect

To evaluate the nature of the electrochemical reaction of 80 µM UA, the peak current and the peak potential were investigated by cyclic voltammogram (CV) at different scan rates (10–300 mV s^{-1}) using the modified electrode. It was found that (Fig. 2B) with the increase in scan rate, the peak currents were enhanced without a shift in peak potentials. The inset of Fig. 2B indicates that the peak currents and square root of scan rate (ν½) have a linear relationship with a correlation coefficient (R^2) of 0.99. It can be concluded that the diffusion mechanism controlled the electrode process.

Electrochemical impedance spectroscopy

To examine the electron transfer properties of modified electrodes, the EIS curves of the modified electrodes at each step were tested in 5.0 mM $[Fe(CN)6]^{3-/4-}$ containing 0.1 M KCl with an amplitude of 5.0 mV. The Nyquist plots are shown in Fig. S5A. According to the results, the diameter of the impedance semicircle H-UOX/CPE is higher than that of the CPE, indicating a higher electron-transfer resistance and lower conductivity. The electron-transfer resistance of the H-UOX/Ni-MOF/CPE diminished in comparison to the previous two electrodes, which might be ascribed to the high conductivity of Ni-MOF. The largest diameter of the impedance semicircle was obtained at UOX/CPE, indicating that the UOX decelerated the electron-transfer process. The equivalent electrical circuit corresponding to the Nyquist plots of different electrodes (Fig. S6) and a table of the set of data obtained by these fittings were prepared (Table S1). EIS was accomplished within the frequency range of 100 mHz–100 kHz with an amplitude of 10 mV.

Optimization

To obtain maximum responses toward uric acid, the experimental parameters, including pH (Fig. S7A) and type of buffer (Fig. S7B), Ni-MOF percentage (Fig. S7C), and concentration of buffer (Fig. S7D), were optimized and shown in supplementary electronic materials.

Analytical performance

Under the optimized parameters, the analytical performance of the suggested biosensor was investigated in terms of linear range, the limit of detection (LOD), and relative standard deviations (RSDs). DP voltammograms of incremental concentrations of UA were obtained. According to Fig. 2C, it was found that the signal grew by elevating the concentration values from 0.3 to 140.0 µM. Figure 2D and Fig. 2E prove the linear relationship between the different concentrations of UA (0.3–10 and 10–140 µM, respectively) and peak current with the correlation coefficient (R^2) of 0.9971 and 0.9916 and linear regression equation of $I(\mu A) = 0.7841\ C(\mu M) + 0.2249$ and $I(\mu A) = 0.7203\ C(\mu M) + 1.3596$, respectively. We set the standard deviation of blank determinations (sb) to 0.022 and used 3sb/m (where m = 0.7841 is a slope of the calibration plot in range of 0.3–10 µM) to obtain

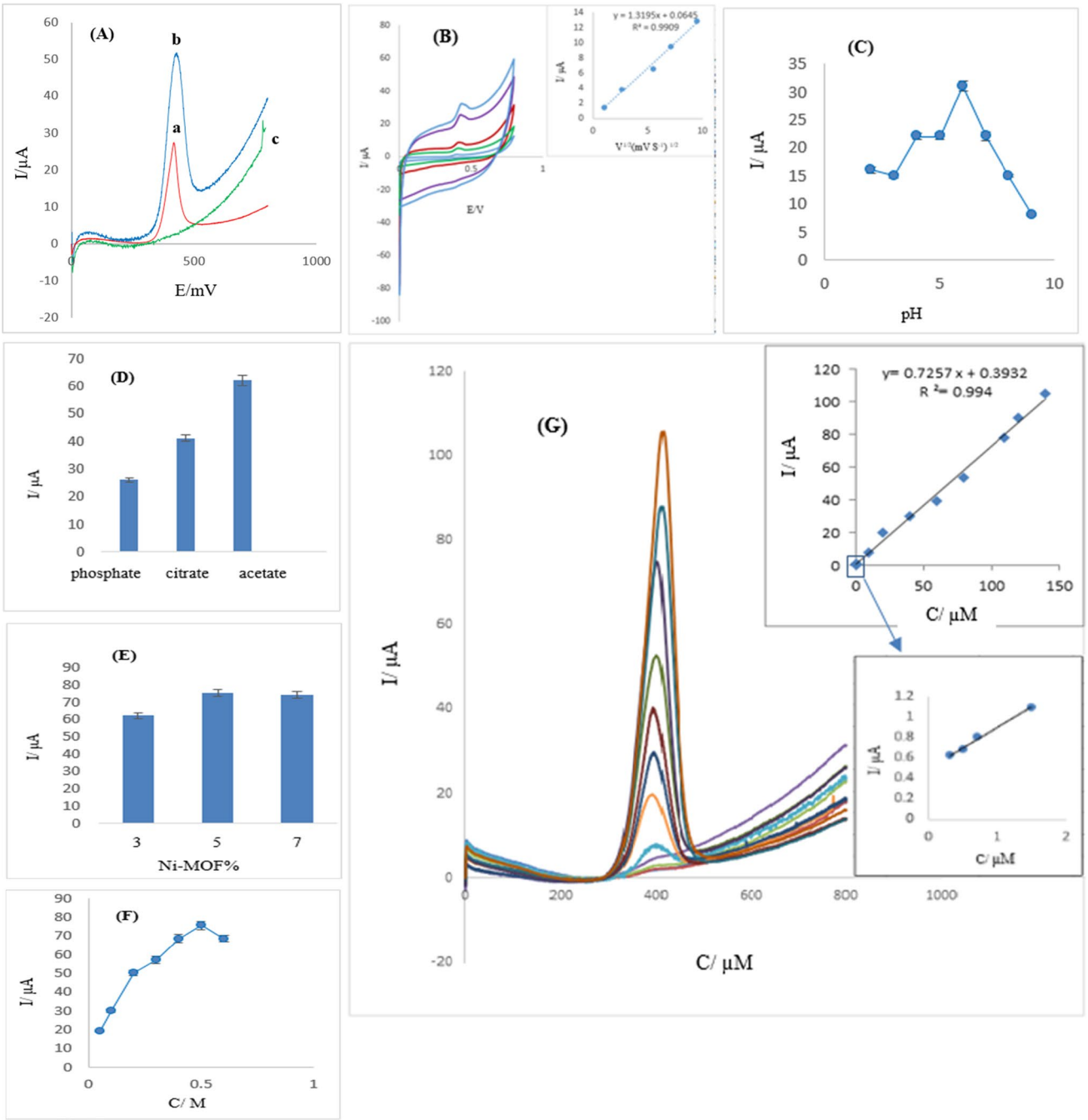

Fig. 2 (**A**) DP voltammograms of (a) CPE, (b) H-UOX/CPE, (c) H-UOX/Ni-MOF/CPE (from an 80 µM UA), and (d) H-UOX/Ni-MOF/CPE (from an 0.50 M acetate buffer (0 µM UA)). (**B**) The CVs of 80 µM UA in 0.5 M acetate buffer (pH 5.5) at different scan rates (10, 20, 30, 40, 50, 60, 70 ….0.300 mV $s.^{-1}$). Inset: relationship between the oxidation peak current and the square root of scan rate (ν½). (**C**) DP voltammograms of UA at H-UOX/Ni-MOF/CPE at different concentrations of UA (down to up: 0, 0.30, 0.50, 0.70, 1.5, 10.0, 20.0, 40.0, 60.0, 80.0, 110.0, 120.0, 140.0 µM). (**D**) Linear relationship of oxidation peak currents vs. concentration of UA (0.30, 0.50, 0.70, 1.5, 10.0 µM). (**E**) Linear relationship of oxidation peak currents vs. concentration of UA (10.0, 20.0, 40.0, 60.0, 80.0, 110.0, 120.0, 140.0 µM) (in all experiments, each point was tested for three times, $n = 3$)

LOD = 0.084 µM. The repeatability of the biosensor was investigated with six replicate measurements of 2 µM UA which resulted in RSDs of 3.06%. The reproducibility of the proposed method was also investigated in six independent measurements using six separate electrodes prepared under the same fabrication conditions. The enzyme was prepared in one batch. The corresponding RSDs were computed as 4.90%. A comparison of the LOD and linear range between

Table 2 Comparison of analytical performance of the biosensor with other methods reported for the detection of UA

Analytical method	Linear range (μM)	Detection limit (μM)	References
UOx[a]@MOF/BNSs-DOX[b]/GCE	0.1–200	0.025	[47]
UOx@MOF(AuNC)/GCE	0.1–10, 10–300	0.02	[48]
CNCo/GCE	2–110	0.83	[7]
MWCNT@FC NFs GCE	0.50–500	0.30	[49]
MWCNT-COOH/SWCNT-OH/GCE	2–150	0.61	[50]
MnO/C/GCE	0.50–14	0.02	[51]
N-Rgo/GCE	1–30	0.20	[52]
laser-engraved wearable sensor	-	0.74	[53]
WS2/GCE	5–1000	1.20	[54]
Nafion/ZnO QDs/UOX/SPE	1000–10,000	22.97	[55]
UOX/MWCNT-CMC/Au	20–5000	2.80	[56]
PEI/P2W17V/CNTs-CS/AuCo/P2W17V/GCE	0.75–100.66	0.25	[57]
		2.86	
Ultrathin g-C_3N_4	10–100	8.90	[58]
H-UOX/Ni-MOF/ CPE	0.30–140	0.09	This work

uox uricase, *BNSs-DOX* boron nanosheets-doxorubicin, *AuNC* hollow gold nanocage, *CNCo/GCE* N,Co-doped porous carbon/glassy carbon electrode, *FC NFs* ferric ceria nanofibers, *MWCNT-COOH/SWCNT-OH* hybrid carbon nanotubes, *MnO/C* carbon-coated MnO, *N-Rgo* nitrogen-doped reduced graphene oxide, *ZnO QDs* ZnO quantum dots, *CMC* carboxymethylcellulose, *CNTs-CS* carbon nanotubes-CS, *g-C_3N_4* graphitic carbon nitride nanosheets

the developed biosensor and previous reports is displayed in Table 2. According to the analytical parameters, the developed H-UOX/Ni-MOF/CPE biosensor is better than or comparable to other sensors previously reported.

Interference and stability studies

The influences of some possible interfering compounds, including ascorbic acid, urea, glucose, dopamine, and L-cysteine on the measurement of UA with the proposed biosensor, were investigated using the detection of 2 μM UA in the absence and presence of interferences. A component that causes more than 5% variation in the biosensor response to UA was considered an interfering substance. The results are presented in Table S2. As can be seen, upon adding ascorbic acid, urea, glucose, dopamine, and L-cysteine (75, 100, 75, 30, and 100 μM, respectively) to 2 μM UA, no considerable change in the peak current of UA occurred. It can be concluded that the proposed biosensor can be used for UA determination in biological samples.

Furthermore, the stability of the biosensor was investigated in the presence of UA (100 μM). The electrode was stored at 4 °C when not in use. After 4 months, the biosensor retained 96% of its activity (Fig. S8A). Thus, no considerable decline was seen in the original peak current for the detection. The observation indicated the excellent long-term stability of the biosensor in comparison to previously reported sensors such as Fc-S–Au/C NC/graphene/GCE [59]. In the case of reusability, the electrode can be used for more than 160 measurements, at the end of which it lost 2% of its initial activity.

Conclusion

A novel electrochemical biosensor, i.e., H-UOX/Ni-MOF/CPE, was developed for UA detection, where the urate oxidase enzyme was successfully applied in the CPE using Ni-MOF. The affinity between histidine and Ni was applied for the first time in this work, which provided a favorable environment for urate oxidase retaining in the proper direction. This biosensor thus obtained is an easy and fast method for UA determination and can be used for healthcare monitoring in clinical applications. In addition, it shows sensitive biosensing for uric acid with excellent selectivity and reusability (more than 160 measurements) (Fig. S8B), and has the advantage of easy fabrication and low-cost detection. It was utilized for the detection of UA in a real sample with good accuracy. Detection values for a real sample (serum) revealed good agreement with the results obtained by a clinical analytical method (ELISA method). This biosensor could be applicable to the clinical need for convenient and frequent uric acid detection and assist in improving the diagnosis of metabolic diseases such as gout. The procedure may be easily extended to other biosensors. Nonetheless, the reproducibility of the proposed biosensor is not very good and needs to be improved for more clinical applications.

Supplementary Information The online version contains supplementary material available at https://doi.org/10.1007/s00604-022-05408-0.

Acknowledgements The authors would like to dedicate the present dissertation to the late Mr. Alireza Afzalipour and Mrs. Fakhereh Saba, the founders of the University of Kerman, because of their foresight and generosity in establishing this institution to train future generations of scientists. In addition, the authors acknowledge their appreciation to the late Dr. Parviz Dabiri for his generous support in establishing our research laboratory.

Declarations

Conflict of interest The authors declare no competing interests.

References

1. Plausinaitis D, Sinkevicius L, Samukaite-Bubniene U, Ratautaite V, Ramanavicius A (2020) Evaluation of electrochemical quartz crystal microbalance based sensor modified by uric acid-imprinted polypyrrole. Talanta 220:121414
2. Zhang W, Liu L, Lia Y, Wang D, Ma H, Ren H, Shi Y, Han Y, Ye BC (2018) Electrochemical sensing platform based on the biomass-derived microporous carbons for simultaneous determination of ascorbic acid, dopamine, and uric acid. Biosens Bioelectron 121:96–43
3. Ivekovic D, Japec M, Solar M, Zivkovic N (2012) Amperometric uric acid biosensor with improved analytical performances based on alkaline-stable H2O2 transducer. Int J Electrochem Sci 7:3252–3264
4. Liu L, Liu L, Wang Y, Ye BC (2019) A novel electrochemical sensor based on bimetallic metal–organic framework-derived porous carbon for detection of uric acid. Talanta 199:478–484
5. Saqib M, Qi L, Hui P, Nsabimana A, Halawa M, Zhang W, Xu G (2018) Development of luminol-N-hydroxyphthalimide chemiluminescence system for highly selective and sensitive detection of superoxide dismutase, uric acid and Co 2+. Biosens Bioelectron 99:519–524
6. Vakh C, Koronkiewicz S, Kalinowski S, Moskvin L, Bulatov A (2017) An automatic chemiluminescence method based on the multi-pumping flow system coupled with the fluidized reactor and direct-injection detector: determination of uric acid in saliva samples. Talanta 167:725–732
7. Dai X, Fang X, Zhang C, Xu R, Xu B (2007) Determination of serum uric acid using high-performance liquid chromatography (HPLC)/isotope dilution mass spectrometry (ID-MS) as a candidate reference method. J Chromatogr B 857:287–295
8. Xu P, Li R, Tu Y, Yan J (2015) A gold nanocluster-based sensor for sensitive uric acid detection. Talanta 144:704–709
9. Bi H, Li Y, Lio S, Guo P, Wei Z, Lv C, Zhang J, Zhao XS (2012) Carbon-nanotube-modified glassy carbon electrode for simultaneous determination of dopamine, ascorbic acid and uric acid: the effect of functional groups. Sens Actuators B: Chem 171–172:1132–1140
10. Erden PE, Kilic E (2013) A review of enzymatic uric acid biosensors based on amperometric detection. Talanta 107:312–323
11. Liu Y, Yuan M, Liu L, Guo R (2013) A facile electrochemical uricase biosensor designed from gold/amino acid nanocomposites. Sens Actuators B: Chem 176:592–597
12. Ghanbari-Ardestani S, Khojasteh-Band S, Zaboli M, Hassani Z, Mortezavi M, Mahani M, Torkzadeh-Mahani M (2019) The effect of different percentages of triethanolammonium butyrate ionic liquid on the structure and activity of urate oxidase: molecular docking, molecular dynamics simulation, and experimental study. J Mol Liq 292:111318
13. Li W, Xu S, Zhang B, Zhu Y, Hua Y, Kong X, Sun L, Hong J (2017) Directed evolution to improve the catalytic efficiency of urate oxidase from Bacillus subtilis. PLOS ONE 1–18
14. Alakel N, Middeke JM, Schetelig J, Bornhauser M (2017) Prevention and treatment of tumor lysis syndrome, and the efficacy and role of rasburicase. OncoTargets and Ther 10:597–605
15. Pui CH, Mahmoud HH, Wiley JM, Woods GM, Leverger G, Camitta B, Hastings C, Blaney SM, Relling MV, Reaman GH (2001) Recombinant urate oxidase for the prophylaxis or treatment of hyperuricemia in patients with leukemia or lymphoma. Am J Clin Oncol 19:697–704
16. Chen D, Wang Q, Jin J, Wu P, Wang H, Yu S, Zhang H, Cai C (2010) Low-potential detection of endogenous and physiological uric acid at uricase-thioninesingle-walled carbon nanotube modified electrodes. Anal Chem 82:2448–2455
17. Lian X, Fang Y, Joseph E, Wang Q, Li J, Banerjee S, Lollar C, Wang X, Zhou HC (2017) Enzyme–MOF (metal–organic framework) composites. Chem Soc Rev 46:3386–3401
18. Liu X, Qi W, Wang Y, Su R, He Z (2017) A facile enzyme immobilization strategy with high stable hierarchically porous metal-organic frameworks. Nanoscale 9:17561–17570
19. Liu X, Qi W, Wang Y, Lin D, Yang X, Su R, He Z (2018) Rational design of mimic multi-enzyme systems in hierarchically porous biomimetic metal-organic frameworks. ACS Appl Mater Interfaces 10(39):33407–33415
20. Zhou Y, Mao Z, Wang W, Yang Z, Liu X (2016) In-situ fabrication of graphene oxide hybrid Ni-based metal–organic framework (Ni-MOFs@GO) with ultrahigh capacitance as electrochemical pseudocapacitor materials. ACS Appl Mater Interfaces 8(42):28904–28916
21. Stock N, Biswas Sh (2012) Synthesis of metal-organic frameworks (MOFs): routes to various MOF topologies, morphologies, and composites. Chem Rev 112(2):933–969
22. Long JR, Yaghi OM (2009) The pervasive chemistry of metal–organic frameworks. Chem Soc Rev 38:1213–1214
23. Wu CD, Zhao M (2017) Incorporation of molecular catalysts in metal–organic frameworks for highly efficient heterogeneous catalysis. Adv Mater 29:1605446
24. Horcajada P, Serre C, Maurin G, Ramsahye NA, Balas F, Vallet-Regi M, Sebban M, Taulelle F, Ferey G (2008) Flexible porous metal-organic frameworks for a controlled drug delivery. J Am Chem Soc 130(21):6774–6780
25. Horcajada P, Chalati T, Serre C, Gillet B, Sebrie C, Baati T, Eubank JF, Heurtaux D, Clayette P, Kreuz C, Chang JS, Hwang YK, Marsaud V, Bories PN, Cynober L, Gil S, Férey G, Couvreur P, Gref R (2010) Porous metal–organic-framework nanoscale carriers as a potential platform for drug delivery and imaging. Nat Mater 9:172–178
26. Xiao Y, Cui Y, Zheng Q, Xiang S, Qian G, Chen B (2010) A microporous luminescent metal–organic framework for highly selective and sensitive sensing of Cu2+ in aqueous solution. Chem Commun 46:5503–5505
27. Liao FS, Lo WS, Hsu YS, Wu CC, Wang SC, Shieh FK, Morabito JV, Chou LY, Wu KCW, Tsung CK (2017) Shielding against unfolding by embedding enzymes in metal− organic frameworks via a de novo approach. J Am Chem Soc 139(19):6530–6533
28. Motamedi A, Barani M, Lohrasbi-Nejad A, Mortazavi M, Riahi-Medvar A, Varma RS, Torkzade-Mahani M (2021) Enhancement of thermostability of Aspergillus flavus urate oxidase by immobilization on the Ni-based magnetic metal–organic framework. Nanomaterials 11(7):1759
29. Ravikumar R, Chen LC, Jayaraman P, Poh CL, Chan CC (2017) Chitosan-nickel film based interferometric optical fiber sensor

for label free detection of histidine tagged proteins. Biosens Bioelectron 99:578–585
30. Chang AY, Chau V, Landas JA, Pang Y (2017) Preparation of calcium competent Escherichia coli and heat-shock transformation. JEMI methods 1:22–25
31. Taherimehr Zahra, Zaboli Maryam, Torkzadeh-Mahani Masoud (2020) New insight into the molecular mechanism of the trehalose effect on urate oxidase stability. J Biomol Struct Dyn 4:1461–1471
32. Zaboli M, Saeidnia F, Zaboli M, Torkzadeh-Mahani M (2021) Stabilization of recombinant d-Lactate dehydrogenase enzyme with trehalose: response surface methodology and molecular dynamics simulation study. Process Biochemi 101:26–35
33. Bradford MM (1976) A rapid and sensitive method for the quantification of microgram quantities of protein utilizing the principle of protein-dye binding. Anal Biochem 72(1–2):248–254
34. Manivel P, Suryanarayanan V, Nesakumar N, Velayutham D, Madasamy K, Kathiresan M, Kulandaisamy AJ, Rayappan JBB (2018) A novel electrochemical sensor based on a nickel-metal organic framework for efficient electrocatalytic oxidation and rapid detection of lactate. New J Chem 42:11839–11846
35. Phan NTS, Nguyen TT, Ta AH (2012) The arylation of aldehydes with arylboronic acids using metal-organic framework Ni(HBTC) BPY as an efficient heterogeneous catalyst. J Mol Catal A Chem 365:95–102